Electronic Supplementary Material (ESI) for Journal of Materials Chemistry A.

Integrating the multi-functionalities in metalloporphyrin porous organic polymers enabling strong polysulfide anchors and rapid electrochemical kinetics in Li-S battery

Yun Sheng Ye*, Mohamed Gamal Mohamed, Cheng Wei Chen, and Shiao Wei Kuo*

Department of Materials and Optoelectronic Science, National Sun Yat-sen University, Kaohsiung, 80424, Taiwan

E-mail: ysye@mail.nsysu.edu.tw; kuosw@faculty.nsysu.edu.tw.

Experimental

Materials

4-nitrobenzaldehyde (98%, Sigma-Aldrich), acetic anhydride (≥99%, Sigma-Aldrich), pyrrole (98%, Sigma-Aldrich), propanoic acid (>99.0%, TCI), pyruvaldehyde solution (37%, Sinopharm Chemical Reagent. Co.), pyridine (>99.0%, TCI), hydrochloric acid (HCl, Acros), dichloromethane (CH_2Cl_2, Acros), methyl alcohol (CH_3OH, ≥99.5%, Sinopharm Chemical Reagent. Co.), glacial acetic acid (≥99.5%, Sinopharm Chemical Reagent. Co.), formaldehyde solution [37% (stabilized with MeOH), TCI], magnesium ether bromide ($MgBr_2{\cdot}Et_2O$, 99%, Sigma-Aldrich), N,N-Dimethylformamide (DMF, 99.9%, Aladdin), cobalt(II) acetate (98.0%, Aladdin), graphene nanosheet (GN, diameter: 5~10 μm, thickness: 3~10 nm), poly (vinylidene difluoride) (PVDF, Alfa Aesar), bis(trifluoromethane)sulfonimide lithium salt (LiTFSI, >98%, Adamas), N-methyl-2-pyrroldone (NMP, ≥99%, Aladdin), Li foil (1 mm thickness), sublimed sulfur (S, Alfa Aesar), lithium sulfide (Li_2S, Alfa Aesar), carbon black (CB, Ketjen black EC600JD, Azko Nobel), 1,3-dioxolane (DOL, >98%, TCI), 1,2-dimethoxyethane (DME, >99%, TCI), lithium nitrate ($LiNO_3$, Adamas).

Preparation of Li_2S_6 solution and sulfur cathode

Li_2S_6 solution was prepared by the overnight reaction of Li_2S and S in a molar ratio of 1:5 in a 1:1 vol ratio of DME/DOL. The sulfur cathode was prepared by mixing S (60 wt%), CB (30 wt%), and PVDF (10 wt%) dissolved in anhydrous NMP in a planetary mixer at 1600 rpm for 1 h and then coating the as-prepared slurry

on aluminum foil, followed by solvent evaporation at 60 °C and further dried at 60 °C under vacuum for 12 h. The active material loading in the S-cathode was ≈2.0 mg cm^{-2} for the regular tests and ≈4.0 mg cm^{-2} for high sulfur tests with the same diameter (14 mm).

Preparation of Por-POP/GN, Por(Mg)-POP/GN, and Por(Co)-POP/GN modified separators

The Por-POP/GN, Por(Mg)-POP/GN, and Por(Co)-POP/GN modified separators were prepared by the synthesized materials, GN and PVDF in a weight ratio of 3:1:1 in anhydrous NMP in a mechanically stirring and then coating the slurry on the Celgard, followed by solvent evaporation at 60 °C and further dried at 60 °C under vacuum for 24 h. The mass loading of the coating layer was ≈0.25 mg cm^{-2} for the regular tests.

Electrochemical and battery measurements

Ion conductivity (σ): The *σ* was measured by electrochemical impedance spectroscopy (EIS, frequency 0.1-10^5 Hz) and calculated using the following equation:

$$\sigma = l/(R \times A) \qquad (\mathbf{S1})$$

Which *l* and *A* are the thickness and area of the separator, respectively, and *R* is the bulk Ohmic resistance of the electrolyte.

Cyclic voltammograms (CV): The CV was measured by inserting the Celgard and modified separators between the S-cathode and Li metal packed in a CR2032 type coin battery in the voltage range of 1.5-3 V at 30 °C and a scan rate of 0.2 mV s^{-1}.

Li-ion diffusion coefficient (D_{Li+}): The D_{Li+} was evaluated by a series of CV scans with various scan rates from 0.1 to 0.5 mV s^{-1} and calculated by the Randles-Sevick equation (eq. S2) as follows:

$$I_P = 2.69 \times 10^5 n^{3/2} A D_{Li+}^{1/2} C_{Li+} v^{1/2} \qquad (S2)$$

In which I_p is the peak current, *n* is the number of electrons transferred in the reaction ($S + 2Li^+ + 2e^- \leftrightarrow Li_2S$, n = 2 for Li-S batteries), *A* is the electrode area, D_{Li+} is the Li-ion diffusion coefficient, C_{Li+} is the change in the concentration of Li-ion, and *v* refers to the scan rate.

Linear sweep voltammetry (LSV): The LSV was measured by inserting the Celgard and modified separators between a stainless steel disc and Li mental packed in a CR2032 type coin battery at 30 °C.

Battery measurements: The CR2032 coin-type batteries were assembled by inserting the Celgard and modified separators between S-cathode and Li metal in an argon-filled glove box. The electrolyte contained 1 M LiTFSI and 1 wt% $LiNO_3$ in a 1:1 vol ratio of DME/DOL. The electrolyte/sulfur (E/S) ratio was 10 mL mg^{-1}. All battery performance was measured in an oven at 30 °C.

Characterization

The samples were characterized by scanning electron microscopy (SEM) and energy-dispersive X-ray spectroscopy (EDX) elemental mapping (FEI Nova NanoSEM450). Transmission electron microscopy (TEM, JEOL JEM-1200CX-II). Thermogravimetric analysis (TGA, Q50) from room temperature to 800 °C at a heating rate of 10 °C min^{-1} under N_2 atmosphere. The Fourier transform infrared spectroscopy (FTIR, Nicolet Avatar 320 FTIR spectrometer). The coating thickness was measured by a stylus profiler (DektakXT, Bruker). UV-Visible spectra were measured by an Evolution 220. X-ray photoelectron spectroscopy (XPS, ESCA 2000 using a monochromatized Al Kα anode). The crystal structure was examined by the X-ray diffraction (XRD) pattern on a PANalytical X'Pert PRO diffractometer equipped with Cu Kα radiation. The electrolyte contact angles were captured by an optical contact-angle measuring device (JC2000C1). Frequency sweeps in the range of 0.1-100 rad s^{-1} were conducted at a shear strain of 0.05% within the linear viscoelastic region of each sample. The electrochemical testing was measured by an AUTO LAB impedance analyzer. The battery performance was measured by LAND Electronic Co., Ltd battery test system at 30°C.

Density functional theory (DFT) calculations

All DFT calculations were conducted using Vienna *ab initio* simulation package (VASP) with exchange-correlation functional of generalized gradient approximation (GGA) of the Perdew-Burke-Ernzerhof (PBE) method. The projected augmented wave (PAW) potential was used to describe the ionic cores and take valence electrons into account using a plane wave basis set with a kinetic energy cut-off of 400 eV. Partial occupancies of the Kohn-Sham orbitals were allowed using the Gaussian smearing method and a width of 0.05 eV. The electronic energy was considered to be self-consistent when the change in energy was less than 10^{-6} eV. Geometry optimization was considered convergent when the change in energy was less than 0.05 eV $Å^{-1}$. Additionally, for the Co atoms, the *U* schemes needed to be applied, and the *U* was set at 3.17 eV. A

large poly-aromatic hydrocarbon (PAH) molecule of $C_{96}H_{24}$ was used to represent graphene in a 30×30×20 Å^3 supercell. The adsorption energies (E_{ads}) were calculated according to equ (S3): $E_{ads} = E_{ad/sub} - E_{ad} - E_{sub}$.

Where $E_{ad/sub}$, E_{ad}, and E_{sub} are the total energies of the optimized adsorbate/substrate system, the adsorbate in the gas phase, and the clean substrate, respectively.

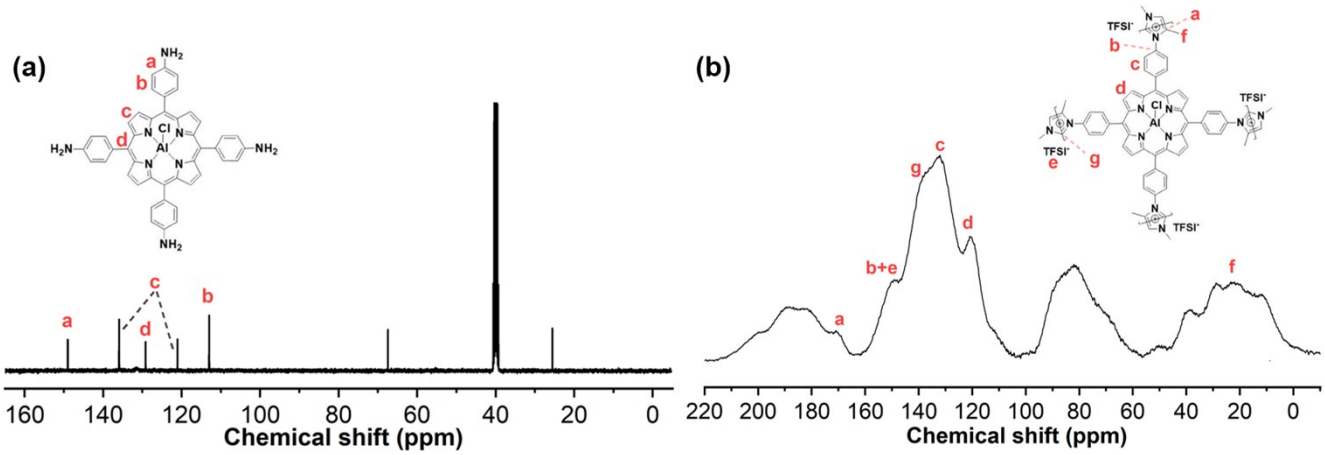

Figure S1. ^{13}C NMR spectrum of (a) TAPP and (b) Por-POP.

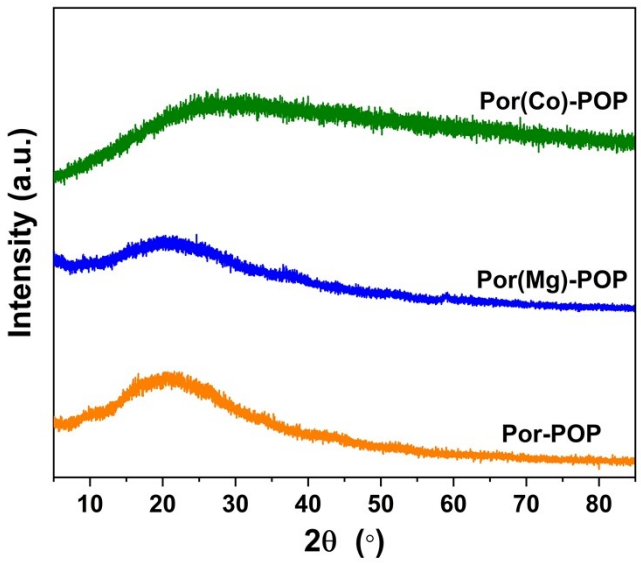

Figure S2. XRD spectra of Por-POP, Por(Mg)-POP, and Por(Co)-POP.

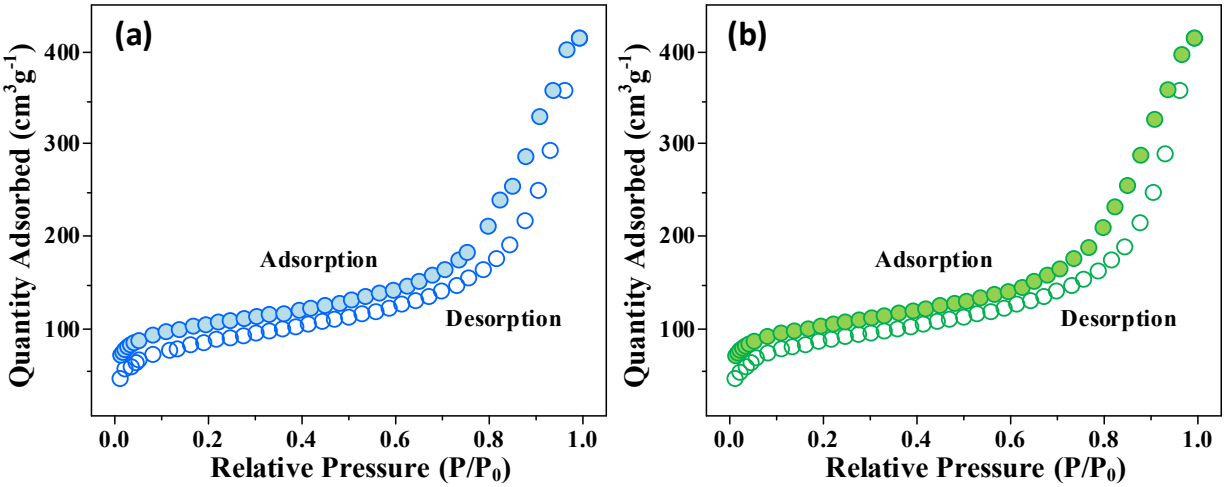

Figure S3. N_2 adsorption-desorption isotherms of (a) Por(Mg)-POP and (b) Por(Co)-POP.

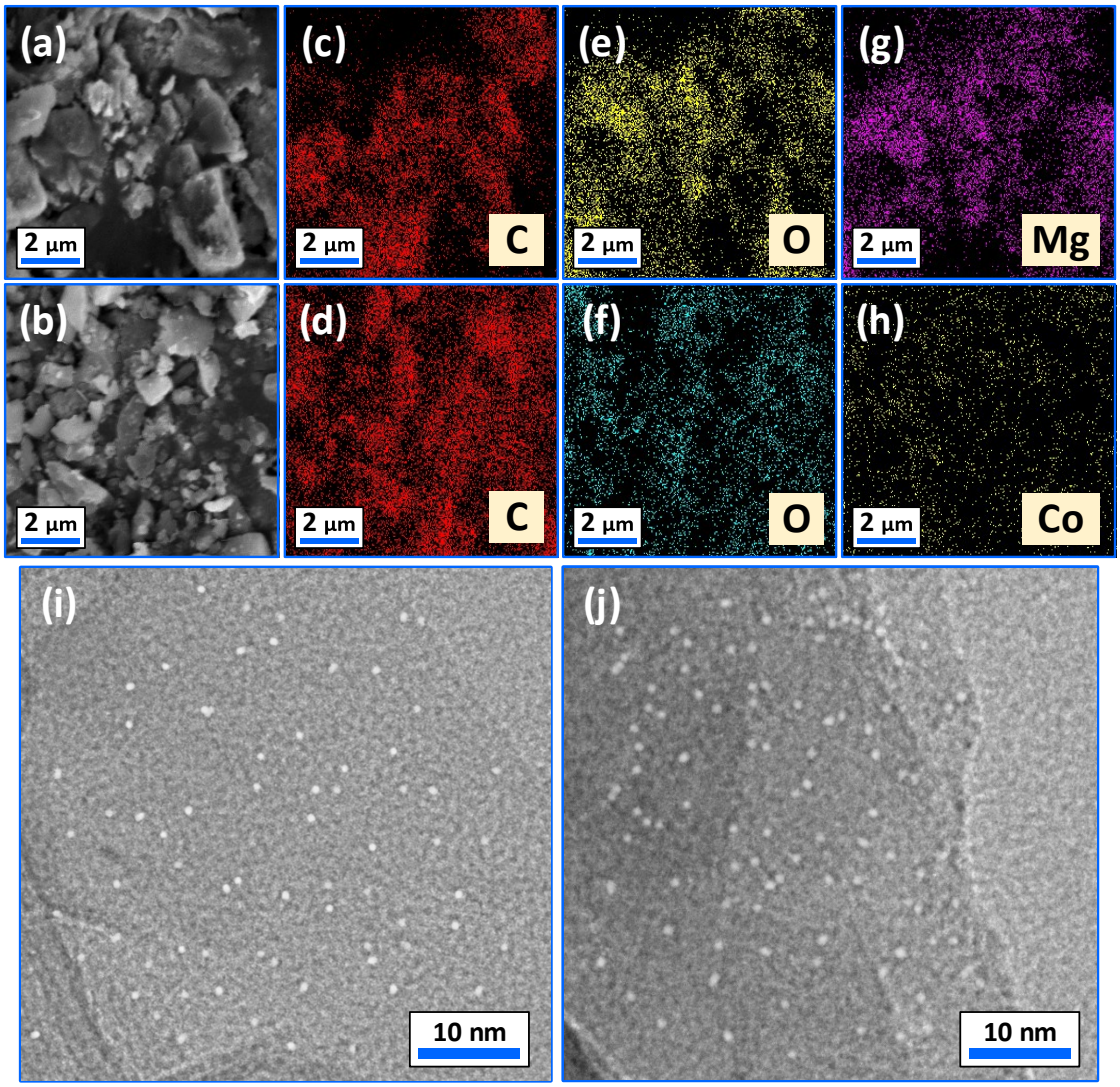

Figure S4. SEM images of (a) Por(Mg)-POP and (b) Por(Co)-POP and corresponding EDS mapping of (c, d) C, (e, f) O, (g) Mg, and (h) Co, respectively; TEM images of (i) Por(Mg)-POP and (j) Por(Co)-POP.

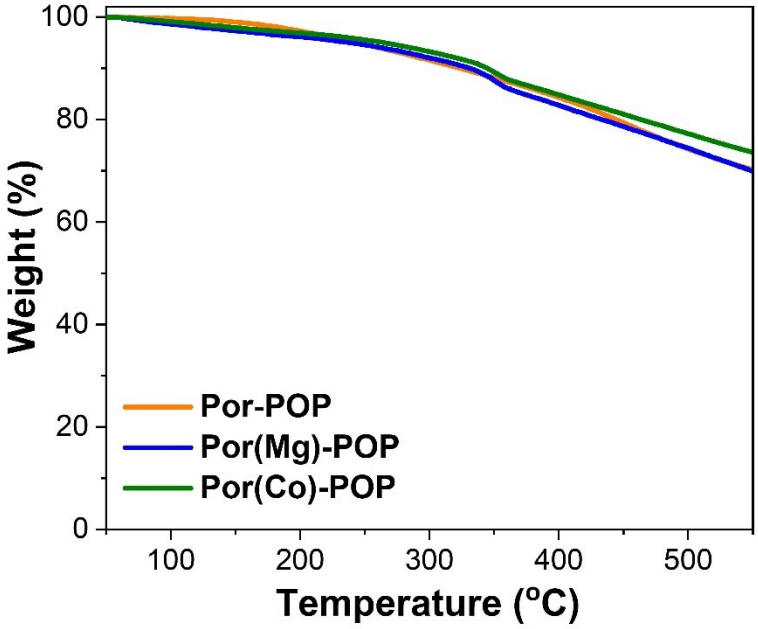

Figure S5. TGA curves of Por-POP, Por(Mg)-POP, and Por(Co)-POP.

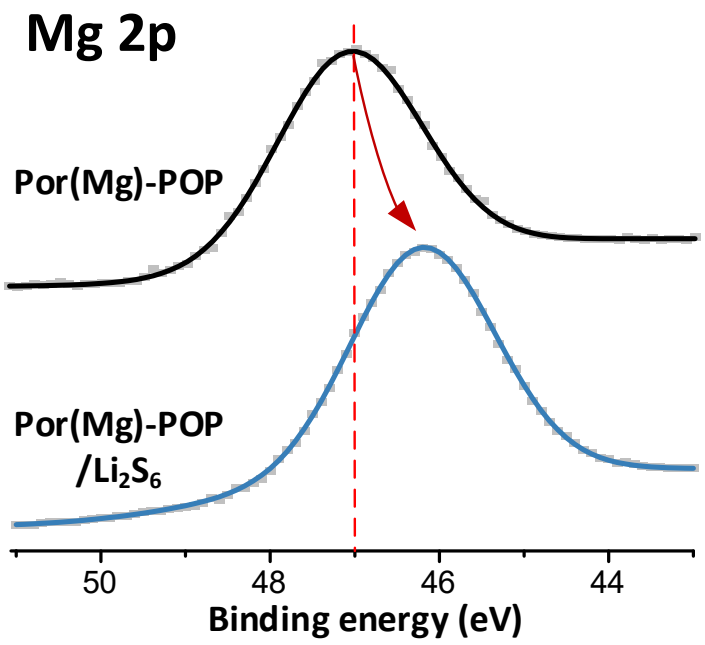

Figure S6. XPS Mg 2p spectra of Por(Mg)-POP.

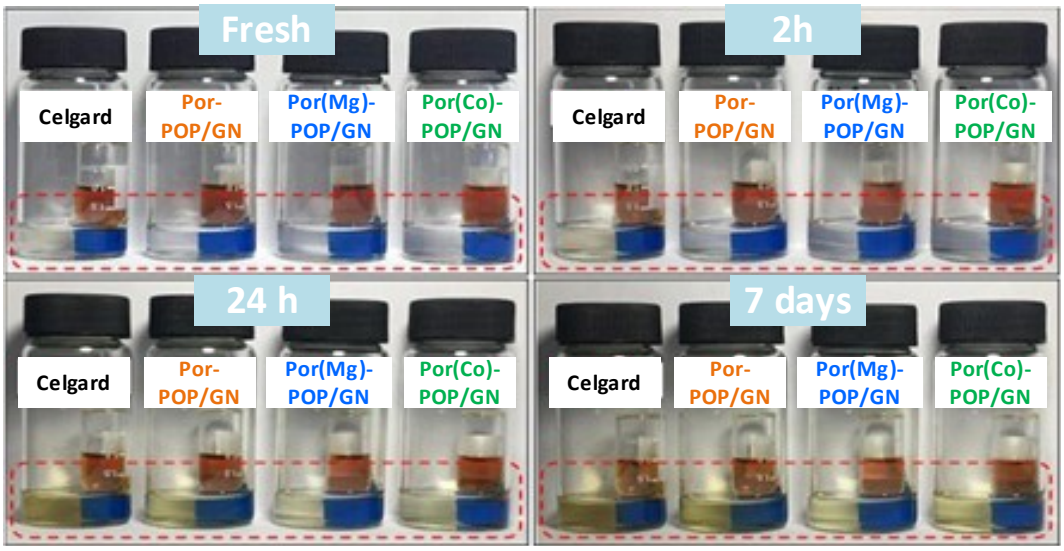

Figure S7. Visualization schematic of Li_2S_6 diffusion with various modified separators after different resting times.

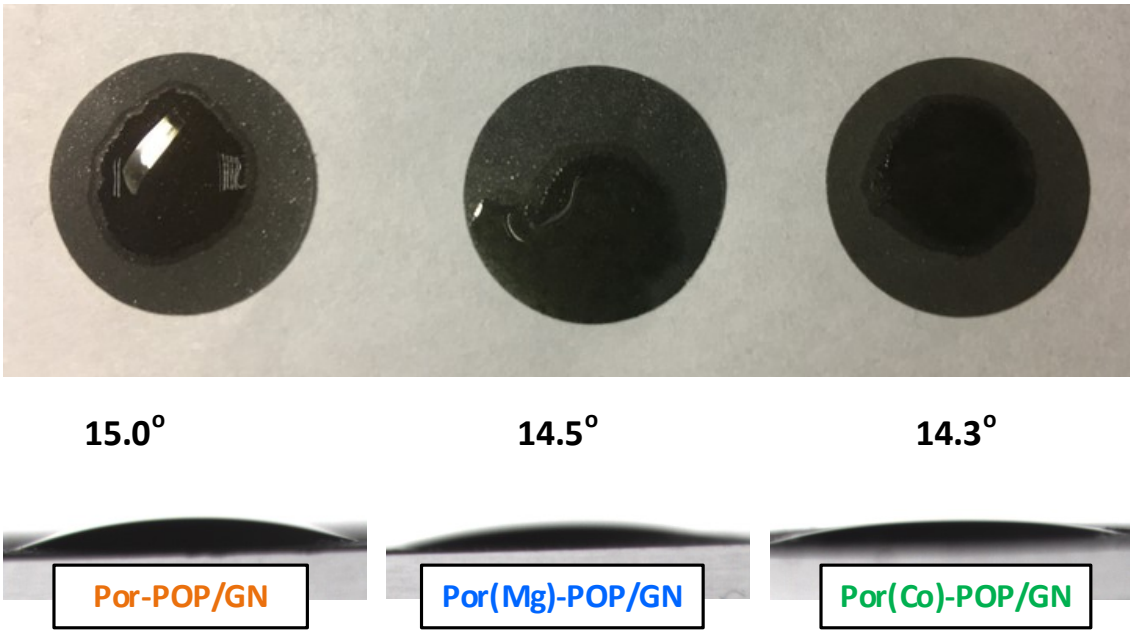

Figure S8. Electrolyte droplets of the modified separators.

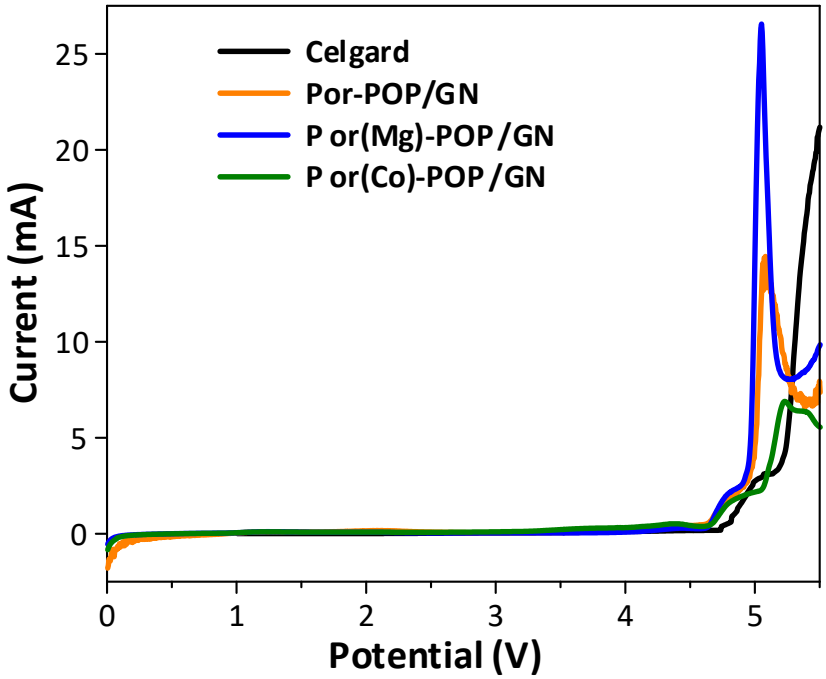

Figure S9. LSV plots of the cell with Celgard and modified separators.

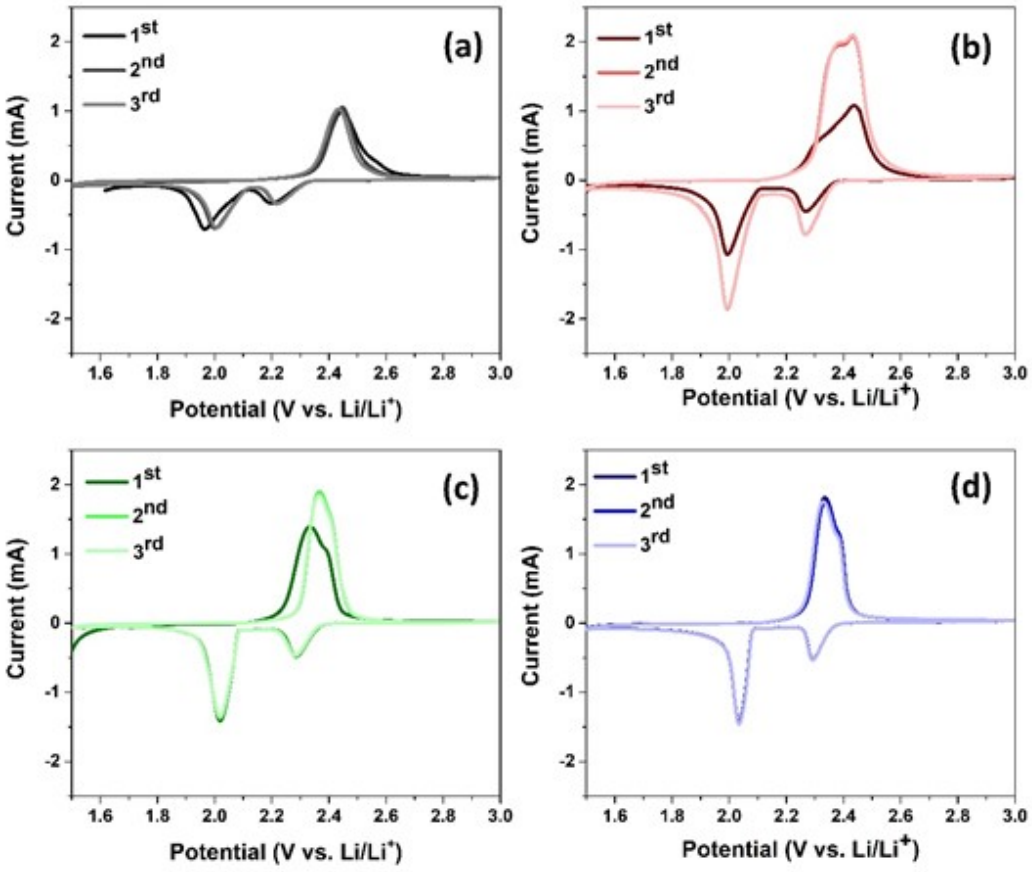

Figure S10. CV profiles of the cells using the (a) Celgard, (b) Por-POP/GN, (c) Por(Mg)-POP/GN, and (d) Por(Co)-POP/GN modified separators.

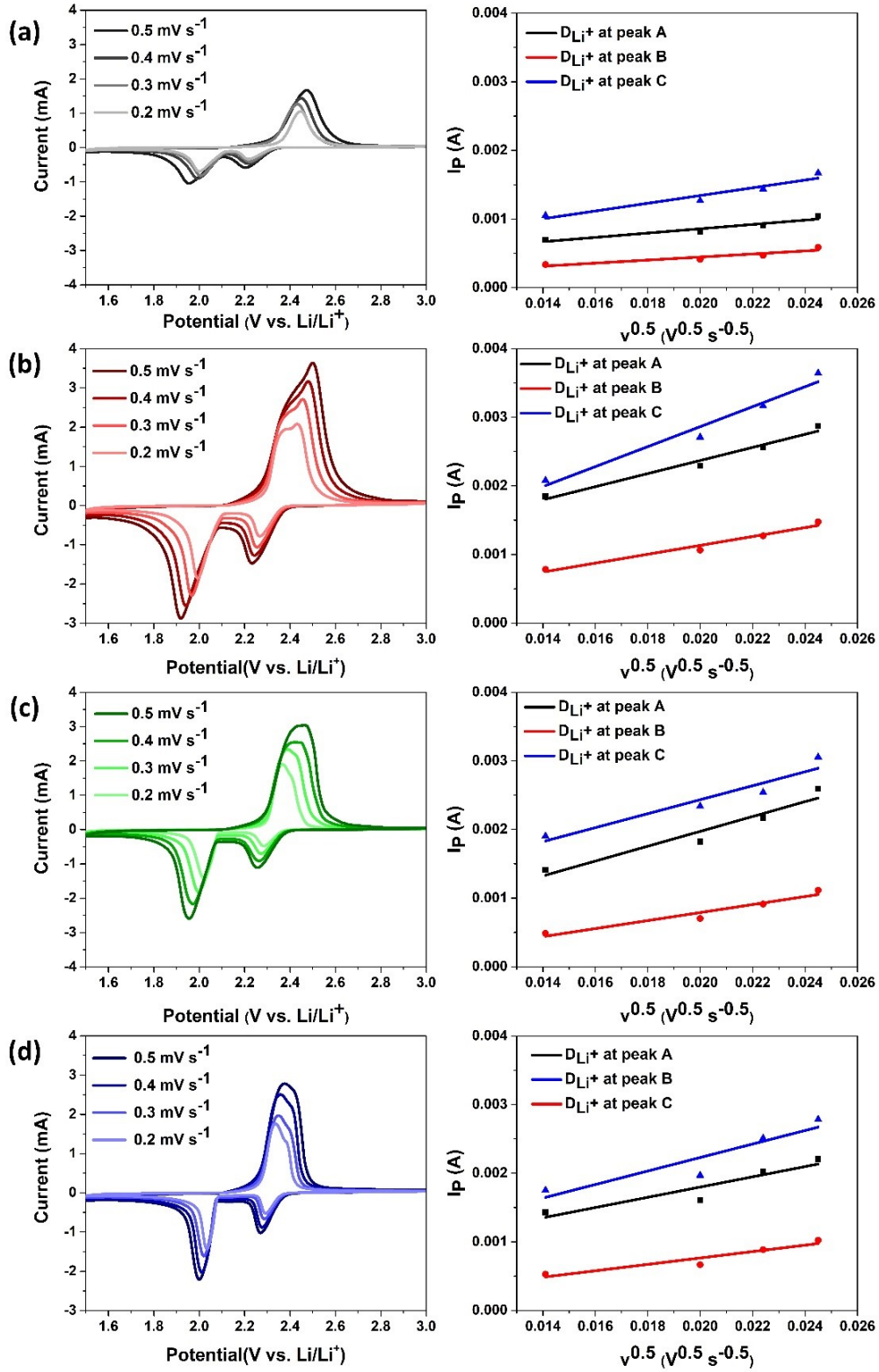

Figure S11. Cyclic voltammograms at various voltage scan rates and corresponding linear fits of the peak current of cells with the (a) Celgard, (b) Por-POP/GN, (c) Por-(Mg)-POP/GN, and (d) Por(Co)-POP/GN modified separators.

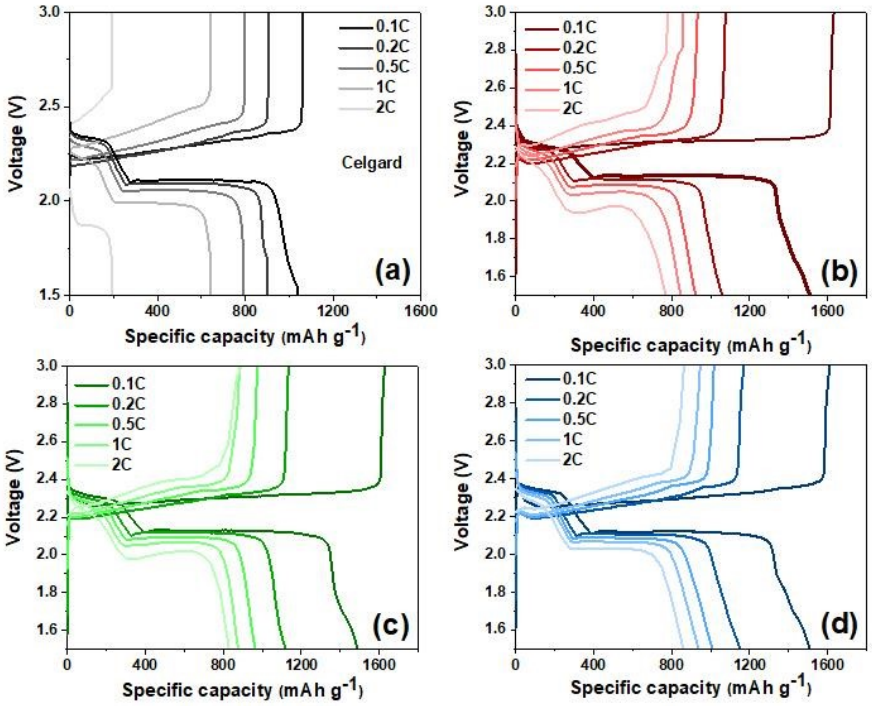

Figure S12. Galvanostatic charge/discharge curves of cells with the (a) Celgard, (b) Por-POP/GN, (c) Por(Mg)-POP/GN, and (d) Por(Co)-POP/GN modified separators at various rates.

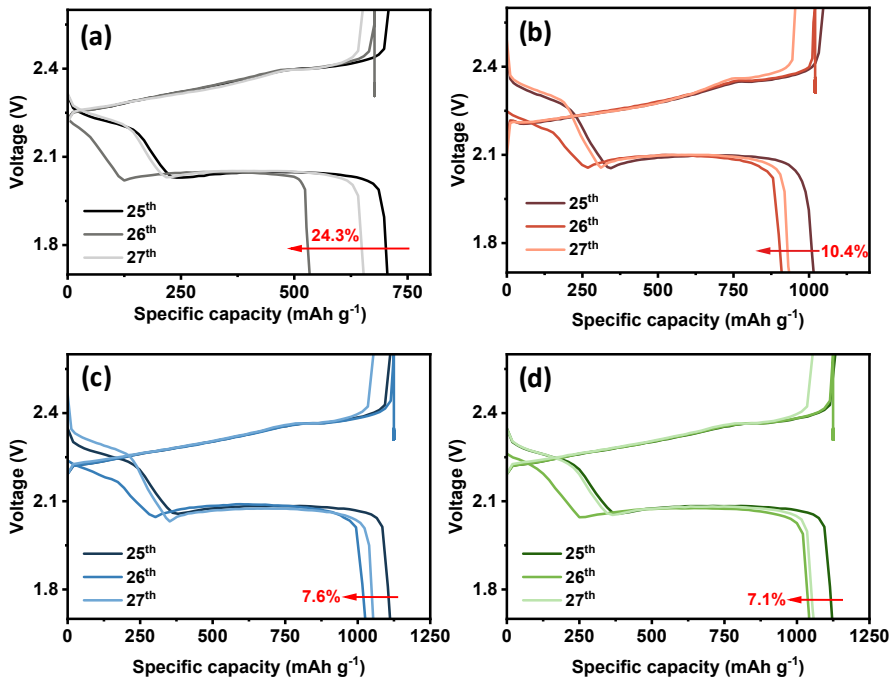

Figure S13. The charge-discharge curves of cells with the (a) Celgard, (b) Por-POP/GN, (c) Por(Mg)-POP/GN, and (d) Por(Co)-POP/GN modified separators at 25^{th}-27^{th} cycles by discharge to 1.5 V and then rest for 72 h.

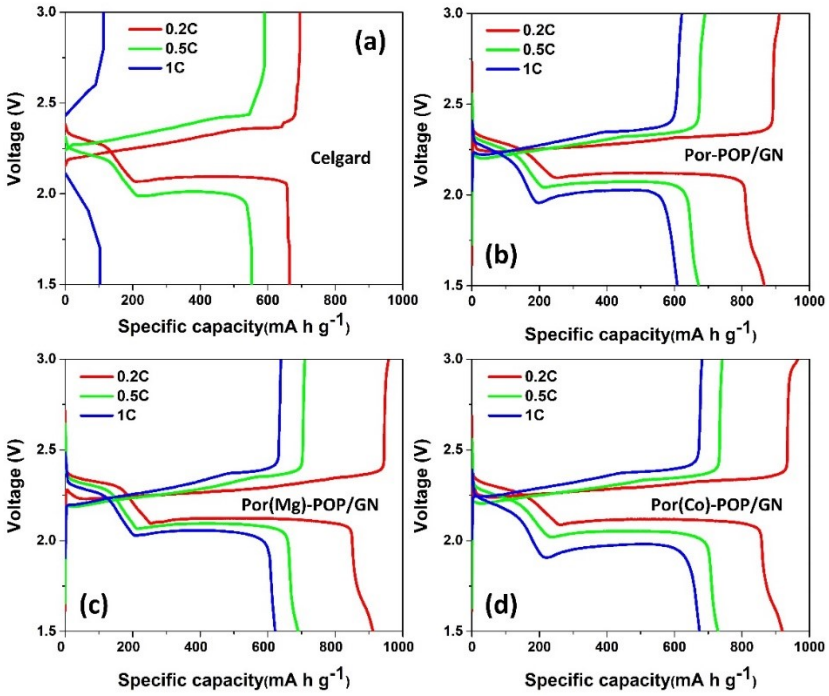

Figure S14. The charge-discharge curves of the (a) Celgard, (b) Por-POP/GN, (c) Por(Mg)-POP/GN, and (d) Por(Co)-POP/GN modified separators with high-sulfur loading at the rates of 0.2, 0.5 and 1 C.

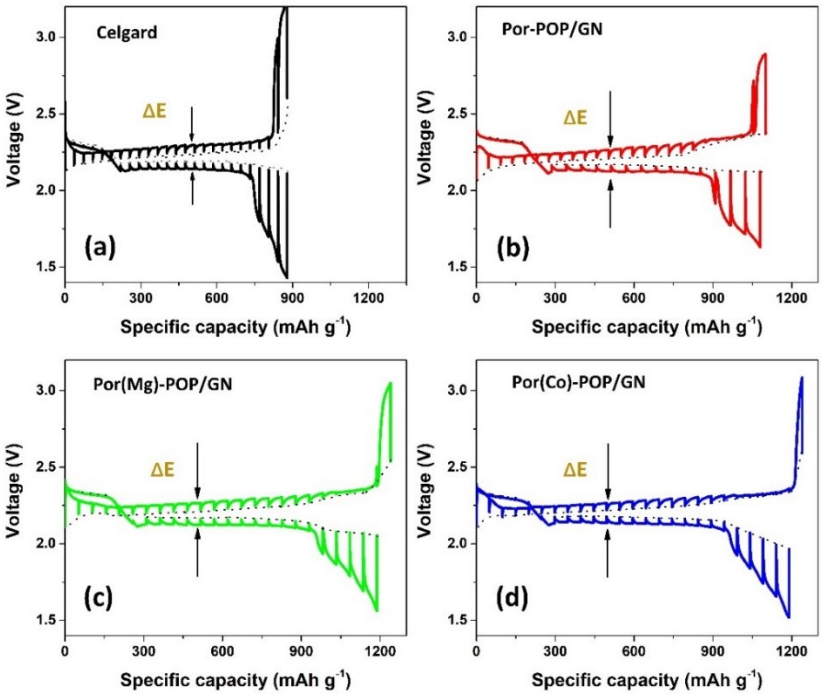

Figure S15. The GITT profiles during the charge/discharge process of the (a) Celgard, (b) Por-POP/GN, (c) Por(Mg)-POP/GN, and (d) Por(Co)-POP/GN modified separators.

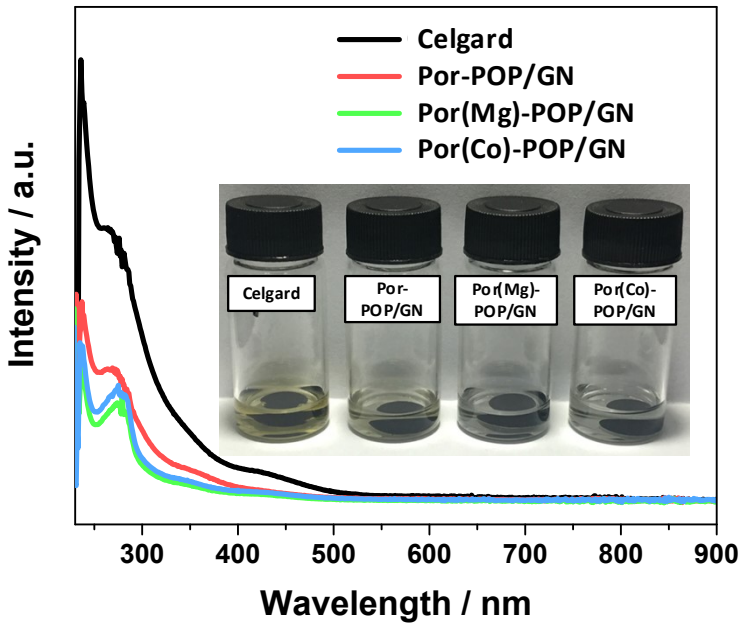

Figure S16. The color change in the THF solution and corresponding UV-vis spectra of the cycled cells with Celgard and modified separators.

Table S1. The electrolyte uptake (*EU*) and electrolyte retention (*ER*) of the Celgard and modified separators.

Parameters	***Celgard***	***Por-POP/GN***	***Por(Mg)-POP/GN***	***Por(Co)-POP/GN***
EU (%)	70.8	172.5	173.9	173.4
ER (0.5 h %)	98.2	99.6	99.5	99.2
ER (1 h %)	95.1	98.7	98.3	98.7
ER (12 h %)	93.4	96.8	96.7	96.4

The *EU* was estimated by soaking weighed the Celgard and modified separators in the electrolyte at 30 ^{o}C for 1 h. The *EU* values were determined by:

$$EU\ (\%) = (W_S - W_I)/W_I \times 100\ \% \quad \text{(S4)}$$

Where W_I and W_S are the weight of the initial Celgard and modified separators after soaking in the electrolyte, respectively.

The *ER* was determined by setting soaked separators in an oven at 30 ^{o}C for 0.2, 0.5, and 12 h. The *ER* values were calculated by:

ER (%) = 100 % - (W_S - W_D)/W_S×100 % (S5)

Where W_S is the pristine Celgard and modified separators after soaking in the electrolyte; W_D is the weight of the soaked separators after deposition in an oven at 30 ^{o}C.

Table S2. Summary of lithium-ion diffusion coefficients (D_{Li^+}) of cells with the Celgard and modified separators.

Parameters	***Celgard***	***Por-POP/GN***	***Por(Mg)-POP/GN***	***Por(Co)-POP/GN***
D_{Li^+} ***(peak A)***	4.6 x 10^{-9}	4.2 x 10^{-8}	5.4 x 10^{-8}	2.5 x 10^{-8}
D_{Li^+} ***(peak B)***	2.3 x 10^{-9}	2.0 x 10^{-8}	1.6 x 10^{-8}	1.0 x 10^{-8}
D_{Li^+} ***(peak C)***	1.5 x 10^{-8}	9.9 x 10^{-8}	4.8 x 10^{-8}	4.5 x 10^{-8}

Table S3. Performance of Li-S batteries with multi-functional modifiers and pure S cathode in this study and previously reported studies for the past five years. ("-" means not mentioned).

Modifier	Thickness /mass of modifier (μm /mg cm^{-2})	Method	S-loading (mg cm^{-2})	Initial capacity (mAh g^{-1})	Decaying rate (%)	Cycles	Discharge current	Ref
MoS_2@CF-NRGO	10	Vacuum assistant filtration (VAF)	1.0-1.2	≈1000	0.064	1000	1C	S1
Li-MOF /RGO	1.2 /0.5-0.6		1.2-1.4	-	0.089	600	1C	S2
MOF/RGO					0.103			
Nb_2O_5/RGO	20 /0.1-0.5		1.5	≈1100	0.086	500	≈0.3C	S3
HVS	≈5		≈1.5	1156	0.072	300	0.2C	S4
LNS/CB	≈3.5/0.7		1-1.2	881	0.028	500	1C	S5
CNF	≈20		1-1.5	955	0.11	200	≈0.66C	S6
VOH@PANI /CNT	≈8/≈0.2		2.2	930	0.037	1000	1C	S7
$WN_{0.67}$@NG	5.6/0.3		1.2-1.5	≈900	0.045	800	1C	S8
rGO@MoS_2	≈8/0.24		1.8-2.0	877	0.116	500	1C	S9
$NiCo_2O_4$ /CNF	38/2.0		1.4-1.8	≈920	0.057	500	2C	S10
CoFe@CNFs	132	Interlayer	1.0	-	0.08	500	1C	S11
LMO/SP/NF	70		1.6	1100	0.09	500	1C	S12
CNT@C	40		1.2	-	0.07	400	1C	S13
Pd_3Co /MWCNT	50		≈1.0	953	0.07	300	2C	S14
Al_2O_3 /C@OSi	18		2.0	1035	0.065	1000	1C	S15
ZnS-RGA	8/0.1	Blade Coating	1.5	800	0.1	500	1C	S16
CoFe@NC	≈8/0.38		1.4	≈800	0.059	1000	1C	S17
SVO/AB	1.2 /0.5-0.6		1.5-2.0	949	0.081	500	1C	S18
Ni@C/G	-/≈0.4		2.0	1337.4	0.061	1000	0.5C	S19
$CoSO_4$	12.1	in-situ growth	2.0	807.7	0.075	500	1C	S20
TpPa-SO_3H	0.9		1.0	864	0.050	500	1C	S21
SNFs/PDA	≈2/≈0.075		1.3	982.2	0.025	1000	1C	S22
Por(Mg)-POP/GN	≈8/≈0.25	Blade Coating	≈2.0	1385	0.052	1000	1C	This work
Por(Co)-POP/GN				1391	0.046			

Table S4. Comparison of separator modifier containing single-atoms catalyst (SAC) in Li-S batteries.

Sample	SAC content (wt%)	Application (method)	S-loading (mg cm^{-2})	Cathode (S content)	Rate at 2C (mAh g^{-1})	Decaying rate (%) (cycles/current)	Ref
Ni@NG	4 (Ni)	13.5 µm thickness /0.3 mg cm^{-2} mass loading (blade-coating)	1.5	Li_2S_6 solution (100%)	≈1000	0.044 (500/1C)	S23
Fe/NG	0.54 (Fe)	≈0.1 mg cm^{-2} mass loading (blade-coating)	4.5		≈875	0.022 (750/0.5C)	S24
SC-Co	0.7 (Co)	0.3 mg cm^{-2} mass loading (VAF)	1.2	MWCNTs/S (63%)	810 (3C)	0.086 (300/0.5C)	S25
Co-N-C	2.8 (Co)	≈0.1 mg cm^{-2} mass loading (VAF))	1.0	CNT/S (63%)	1035	0.1 (300/0.5C)	S26
Fe-PNC	1 (Fe)	Host material	1.3	Fe-PNC/S (70%)	≈250	0.2 (300/0.5C)	S27
NC@SA-Co	4.1 (Co)	10 µm thickness /0.45 mg cm^{-2} mass loading (Interlayer)	1.0	C/S (56%)	694	0.058 (700/2C)	S28
SAZ-AF (ZnENC and Bio-MOF-100)	0.039 (Zn)	≈0.1 mg cm^{-2} mass loading (double coating)	1.5	KB/S (80%)	920.7	0.05 (1000/2C)	S29
Por(Mg)-POP/GN	3.8 (Mg)	8 µm thickness /0.25 mg cm^{-2} mass loading (blade-coating)	≈2.0	60%	826.5	0.046 (1000/1C)	This work
Por(Co)-POP/GN	4.4 (Co)				859.5	0.052 (1000/1C)	

Abbreviation: CF-NRGO: nitrogen-doped reduced graphene oxide and carbonized melamine foam; CNF: carbon nanofiber; Fe/NG: nitrogen doped-graphene foam impregnated with Fe; Fe-PNC: Fe-pristine nitrogen-doped carbon; HVS: VS_2 hexagonal nanotowers; Li-MOF: Li-ion inserted metal oxide framework; LMO: Li_xMoO_y; LNS/CB: laponite nanosheets/carbon black; NC: nitrogen-doped carbon nanocube; NC@SA-Co: single-atom cobalt-anchored nitrogen-doped carbon nanosheets; Pa-SO_3H: 2,5-diaminobenzene sulfonic acid; SAZ-AF: single-atom zinc-anionic framework; SC-Co: atomic-cobalt-implanted supramolecule-derived carbon; SNFs/PDA: silicone nano laments/ polydopamine; SVO/AB: nitrogen-doped sheet VO_2/acetylene black; TP: 1,3,5-triformyl phloroglucinol; VOH@PANI/CNT: polyaniline encapsulated amorphous vanadium pentoxide nanowires/carbon nanotube; $WN_{0.67}$@NG: $WN_{0.67}$-embedded N-doped graphene-nanosheets; ZnENC: Zn-decorated embroidered ball-like nitrogen-doped carbon; ZnS-RGA: zinc sulfide quantum dots/reduced graphene aerogel.

References

(S1) Zhang, J.; Xu, G.; Zhang, Q.; Li, X.; Yang, Y.; Yang, L.; Huang, J.; Zhou, G. Mo-O-C Between MoS_2 and Graphene Toward Accelerated Polysulfide Catalytic Conversion for Advanced Lithium-Sulfur Batteries. *Advanced Science* **2022,** *9* (22), 2201579.

(S2) Zhou, M.; Li, Y.; Lei, T.; Chen, W.; Rao, G.; Xue, L.; Hu, A.; Fan, Y.; Huang, J.; Hu, Y.et al. Ion-Inserted Metal-Organic Frameworks Accelerate the Mass Transfer Kinetics in Lithium-Sulfur Batteries. *Small* **2021,** *17* (44), 2104367.

(S3) Guo, P.; Sun, K.; Shang, X.; Liu, D.; Wang, Y.; Liu, Q.; Fu, Y.; He, D. Nb_2O_5/RGO Nanocomposite Modified Separators with Robust Polysulfide Traps and Catalytic Centers for Boosting Performance of Lithium-Sulfur Batteries. *Small* **2019,** *15* (40), 1902363.

(S4) Wang, J.; Yi, S.; Liu, J.; Sun, S.; Liu, Y.; Yang, D.; Xi, K.; Gao, G.; Abdelkader, A.; Yan, W.et al. Suppressing the Shuttle Effect and Dendrite Growth in Lithium-Sulfur Batteries. *ACS Nano* **2020,** *14* (8), 9819.

(S5) Yang, Y.; Zhang, J. Highly Stable Lithium-Sulfur Batteries Based on Laponite Nanosheet-Coated Celgard Separators. *Advanced Energy Materials* **2018,** *8* (25), 1801778.

(S6) Kong, L.; Fu, X.; Fan, X.; Wang, Y.; Qi, S.; Wu, D.; Tian, G.; Zhong, W.-H. A Janus nanofiber-based separator for trapping polysulfides and facilitating ion-transport in lithium-sulfur batteries. *Nanoscale* **2019,** *11* (39), 18090.

(S7) Chen, K.; Zhang, G.; Xiao, L.; Li, P.; Li, W.; Xu, Q.; Xu, J. Polyaniline Encapsulated Amorphous V_2O_5 Nanowire-Modified Multi-Functional Separators for Lithium-Sulfur Batteries. *Small Methods* **2021,** *5*

(3), 2001056.

(S8) Ma, F.; Yu, B.; Zhang, X.; Zhang, Z.; Srinivas, K.; Wang, X.; Liu, D.; Wang, B.; Zhang, W.; Wu, Q.et al. $WN_{0.67}$-Embedded N-doped Graphene-Nanosheet Interlayer as efficient polysulfide catalyst and absorbant for High-Performance Lithium-Sulfur batteries. *Chemical Engineering Journal* **2022,** *431*, 133439.

(S9) Tan, L.; Li, X.; Wang, Z.; Guo, H.; Wang, J. Lightweight Reduced Graphene Oxide@MoS_2 Interlayer as Polysulfide Barrier for High-Performance Lithium-Sulfur Batteries. *ACS Appl Mater Interfaces* **2018,** *10* (4), 3707.

(S10) Lin, J.X.; Qu, X.M.; Wu, X.H.; Peng, J.; Zhou, S.Y.; Li, J.T.; Zhou, Y.; Mo, Y.X.; Ding, M.J.; Huang, L.et al. $NiCo_2O_4$/CNF Separator Modifiers for Trapping and Catalyzing Polysulfides for High-Performance Lithium-Sulfur Batteries with High Sulfur Loadings and Lean Electrolytes. *ACS Sustainable Chemistry & Engineering* **2021,** *9* (4), 1804.

(S11) Gao, N.; Li, B.; Zhang, Y.; Li, W.; Li, X.; Zhao, J.; Yue, W.; Xing, Z.; Wang, B. CoFe Alloy-Decorated Interlayer with a Synergistic Catalytic Effect Improves the Electrochemical Kinetics of Polysulfide Conversion. *ACS Appl Mater Interfaces* **2021,** *13* (48), 57193.

(S12) Li, T.; Li, Y.; Yang, J.; Deng, Y.; Wu, M.; Wang, Q.; Liu, R.; Ge, B.; Xie, X.; Ma, J. In Situ Electrochemical Activation Derived Li_xMoO_y Nanorods as the Multifunctional Interlayer for Fast Kinetics Li-S batteries. *Small* **2021,** *17* (52), 2104613.

(S13) Dai, Y.; Zheng, W.; Li, X.; Liu, A.; Zhang, W.; Jiang, X.; Wu, X.; Tao, J.; He, G. N-Doped Hierarchically Porous CNT@C Membranes for Accelerating Polysulfide Redox Conversion for High-Energy Lithium-Sulfur Batteries. *ACS Appl Mater Interfaces* **2021,** *13* (2), 2521.

(S14) Cho, S. H.; Cho, S. M.; Bae, K. Y.; Kim, B. H.; Son, B. D.; Yoon, W. Y. Improving electrochemical properties of Lithium-Sulfur batteries by adding a catalyst-embedded interlayer. *Electrochim Acta* **2019,** *315*, 33.

(S15) Chang, C.; Guan, X.; Wang, P.; Zhou, X.; Xie, X.; Ye, Y. Electrically and thermally conductive Al_2O_3/C nanofiber membrane filled with organosilicon as a multifunctional integrated interlayer for lithium-sulfur batteries under lean-electrolyte and thermal gradient. *Chemical Engineering Journal* **2022,** *442*, 135825.

(S16) Liu, Z.; Hu, Z.; Jiang, X.; Zhang, Y.; Wang, X.; Zhang, S. Multi-functional ZnS quantum Dots/Graphene aerogel modified separator for high performance lithium-sulfur batteries. *Electrochim Acta* **2022,** *422*, 140496.

(S17) Wang, Y.; Zhu, L.; Wang, J.; Zhang, Z.; Yu, J.; Yang, Z. Enhanced chemisorption and catalytic conversion

of polysulfides via CoFe@NC nanocubes modified separator for superior Li-S batteries. *Chemical Engineering Journal* **2022,** *433*, 133792.

(S18) Yang, L.; Li, Y.; Wang, Y.; Li, Q.; Chen, Y.; Zhong, B.; Guo, X.; Wu, Z.; Liu, Y.; Wang, G.et al. Nitrogen-doped sheet VO_2 modified separator to enhanced long-cycle performance lithium-sulfur battery. *J Power Sources* **2021,** *501*, 230040.

(S19) Yu, Z.; Wang, B.; Liao, X.; Zhao, K.; Yang, Z.; Xia, F.; Sun, C.; Wang, Z.; Fan, C.; Zhang, J.et al. Boosting Polysulfide Redox Kinetics by Graphene-Supported Ni Nanoparticles with Carbon Coating. *Advanced Energy Materials* **2020,** *10* (25), 2000907.

(S20) Lu, X.; Wang, H.; Liu, X.; Song, Z.; Jiang, N.; Xie, F.; Zheng, Q.; Lin, D. Functional separators prepared via in-situ growth of hollow CoSO4 hydrate arrays on pristine polypropylene membrane for high performance lithium-Sulfur batteries. *J Alloys Compd* **2020,** *838*, 155618.

(S21) Zhao, J.; Yan, G.; Zhang, X.; Feng, Y.; Li, N.; Shi, J.; Qu, X. In situ interfacial polymerization of lithiophilic COF@PP and POP@PP separators with lower shuttle effect and higher ion transport for high-performance Li-S batteries. *Chemical Engineering Journal* **2022,** *442*, 136352.

(S22) Yang, Y.; Wang, W.; Li, L.; Li, B.; Zhang, J. Stable cycling of Li-S batteries by simultaneously suppressing Li-dendrite growth and polysulfide shuttling enabled by a bioinspired separator. *J Mater Chem A* **2020,** *8* (7), 3692.

(S23) Zhang, L.; Liu, D.; Muhammad, Z.; Wan, F.; Xie, W.; Wang, Y.; Song, L.; Niu, Z.; Chen, J. Single Nickel Atoms on Nitrogen-Doped Graphene Enabling Enhanced Kinetics of Lithium-Sulfur Batteries. *Adv Mater* **2019,** *31* (40), 1903955.

(S24) Zhang, K.; Chen, Z.; Ning, R.; Xi, S.; Tang, W.; Du, Y.; Liu, C.; Ren, Z.; Chi, X.; Bai, M.et al. Single-Atom Coated Separator for Robust Lithium-Sulfur Batteries. *ACS Appl Mater Interfaces* **2019,** *11* (28), 25147.

(S25) Xie, J.; Li, B.Q.; Peng, H.J.; Song, Y.W.; Zhao, M.; Chen, X.; Zhang, Q.; Huang, J.Q. Implanting Atomic Cobalt within Mesoporous Carbon toward Highly Stable Lithium-Sulfur Batteries. *Adv Mater* **2019,** *31* (43), 1903813.

(S26) Li, B.Q.; Kong, L.; Zhao, C.X.; Jin, Q.; Chen, X.; Peng, H.J.; Qin, J.L.; Chen, J.X.; Yuan, H.; Zhang, Q.et al. Expediting redox kinetics of sulfur species by atomic-scale electrocatalysts in lithium-sulfur batteries. *InfoMat* **2019,** *1* (4), 533.

(S27) Liu, Z.; Zhou, L.; Ge, Q.; Chen, R.; Ni, M.; Utetiwabo, W.; Zhang, X.; Yang, W. Atomic Iron Catalysis of Polysulfide Conversion in Lithium-Sulfur Batteries. *ACS Appl Mater Interfaces* **2018,** *10* (23), 19311.

(S28) Li, Y.; Zhou, P.; Li, H.; Gao, T.; Zhou, L.; Zhang, Y.; Xiao, N.; Xia, Z.; Wang, L.; Zhang, Q.et al. A

Freestanding Flexible Single-Atom Cobalt-Based Multifunctional Interlayer toward Reversible and Durable Lithium-Sulfur Batteries. *Small Methods* **2020,** *4* (3), 1900701.

(S29) Song, C.L.; Li, Z.H.; Ma, L.Y.; Li, M.Z.; Huang, S.; Hong, X.J.; Cai, Y.P.; Lan, Y.Q. Single-Atom Zinc and Anionic Framework as Janus Separator Coatings for Efficient Inhibition of Lithium Dendrites and Shuttle Effect. *ACS Nano* **2021,** *15* (8), 13436.